International Journal of Optics and Applications 2014, 4(3): 92-100
DOI: 10.5923/j.optics.20140403.04

Analytical Framework to Investigate the Performance of WDM Cascade Demultiplexer

Rasha H. Mahdi[1], R. S. Fyath[2,*]

[1]Department of Laser and Optoelectronics Engineering, Alnahrain University, Baghdad Iraq
[2]Department of Computer Engineering, Alnahrain University, Baghdad, Iraq

Abstract The aim of this paper is to present a framework to analysis the performance of wavelength-division demultiplexers incorporating cascaded stages. Each stage is used as a single-channel drop filter. The analysis is based on the coupled-mode theory (CMT) and takes into account the interaction between successive stages. The CMT is first applied to characterise a single-channel demultiplexer and the results are used to drive expressions for its scattering parameters. Then the analysis is extended to a multi-channel demultiplexer using matrix formulation in order to calculate the scattering parameters related to various ports. Simulation results are presented for two 3-channel demultiplexers, namely (1550, 1300, 850 nm) and (1650, 1550, 1450 nm) demultiplexers. The results reveal that the interaction between successive stages should be taken into account to extract the demultiplexer performance accurately.

Keywords WDM Demultiplexer, Cascade Demultiplexer, Coupled-Mode Theory

1. Introduction

Wavelength-division multiplexing (WDM) is one of the commonly used technologies to increase the capacity of optical communication systems [1-3]. In WDM system, multiple wavelength carriers, each modulated by relatively low bit rate, are grouped (multiplexed) at the transmitter side before launching into the fiber link. At the receiver side, the WDM signal is separated (demultiplexed) to individual wavelengths. Generally, the capacity of WDM system is scaled by the number of used channels (wavelengths). Optical demultiplexers are key components in WDM systems and should be designed carefully to extract the single channel at the base rate where electronics can be used. In the past few years, there has been a tremendous interest in the design of WDM demultiplexers using plasmonic technology [4, 5], photonic crystal technology [6, 7], and silicon photonic platform [8, 9].

One of the simplest methods to design multiple-channel demultiplexers is based on cascade configuration [10-12]. Here the demultiplexer consists of multiple units connected in series; each one is tuned to drop one wavelength (see Fig. 1). Each unit behaves as a narrow bnndpass filter and can be implemented using different techniques.

The design of cascade demultiplexer usually relies heavily on the design of one unit and then projects the results on other units after taking wavelength scaling into account. In this design scenario, each unit is assumed to be not interfered with the neighbouring units. This assumption is justified when the channel spacing is much larger than the bandwidth of the filtering action of each unit. If this assumption is not valid, then more accurate analysis is required to investigate the performance of the cascade demultiplexer. This issue is addressed in this paper where analytical framework based on coupled-mode theory (CMT) is presented to characterise the WDM cascade demultiplexer. The CMT is used to track the incident and reflected forward and backward waves associated with each unit.

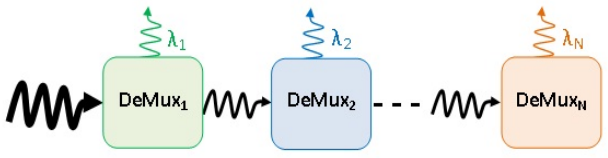

Figure 1. Concept of a cascade demultiplexer. DeMux*i* represents the *i*th unit used to drop the *i*th wavelength λ*i*

Without loss of generality, the analytical framework is illustrated for a cascade demultiplexer whose units are designed as channel-drop filter with wavelength selective reflection cavity. This filter structure has been proposed by Ren et al. [13] using photonic crystal platform to enhance the drop efficiency. The concept has recently been used by Lu et al. [14] to design a plasmonic demultiplexer for optical communication systems. The demultiplexer unit consists of a bus waveguide coupled laterally to two cavities as shown in Fig. 2. One cavity is used to realize a

* Corresponding author:
rsfyath@yahoo.com (R. S. Fyath)
Published online at http://journal.sapub.org/optics

resonant tunnelling-based channel drop filtering and the other is used to realize wavelength-selective reflection feedback.

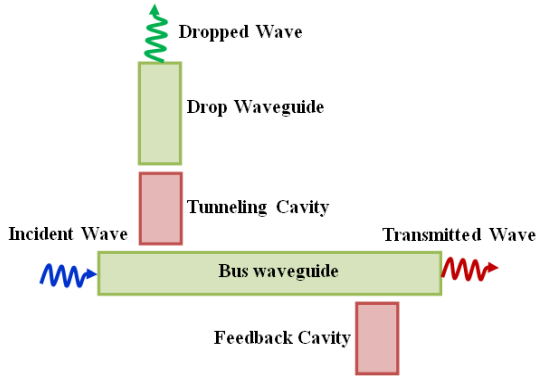

Figure 2. Schematic diagram of a single-channel demultiplexer consisting of a drop nanocavity coupled with a feedback nanocavity

2. Background

This section presents CMT formulation for an optical configuration containing a cavity coupled laterally to a waveguide. The analysis stands heavily on the formulation reported in [15] which has been used widely by other workers [13, 14, 16-20].

2.1. Analysis of Channel Drop Filter Cavity

Figure 3 shows the basic structure of a cavity which is side coupled to a bus waveguide and axially coupled to a drop waveguide. The cavity is used for a resonant tunnelling-based drop operation. The structure is treated as a three-port system with a reference plane passing through the centre of the cavity. It is assumed that the cavity, bus waveguide, and drop waveguide support single mode in the frequency range of interest with negligible nonlinear optics effect. The cavity possesses mirror reflection symmetry with respect to the reference plane. The amplitude of the incoming waves are denoted by s_{+1}, s_{+2} and s_{+3}. The amplitudes of the outgoing waves are denoted by s_{-1}, s_{-2}, and s_{-3}.

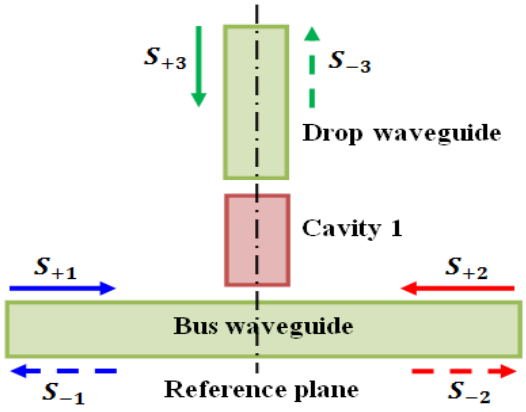

Figure 3. Channel drop filter with cavity 1 used for a resonant tunnelling-based channel drop operation

The time evaluation of the amplitude of the mode in cavity 1 can be expressed as [15, 17, 18]

$$\frac{da}{dt} = (j\omega_{o1} - \frac{\omega_{o1}}{Q_{o1}} - \frac{\omega_{o1}}{2Q_{b1}} - \frac{\omega_{o1}}{2Q_d})a + e^{j\theta_{b1}}\sqrt{\frac{\omega_{o1}}{2Q_{b1}}}s_{+1} + e^{j\theta_{b1}}\sqrt{\frac{\omega_{o1}}{2Q_{b1}}}s_{+2} + e^{j\theta_d}\sqrt{\frac{\omega_{o1}}{Q_d}}s_{+3} \quad (1)$$

where

a = Cavity field amplitude.

ω_{o1}= Resonance frequency of the cavity.

Q_{o1}= Quality factor due to intrinsic loss.

Q_{b1}= Quality factor of the cavity which is connected with rate of decay into the bus waveguide.

Q_d= Quality factor of the cavity which is related to the rate of decay into the drop waveguide.

θ_{b1}= Phase of the coupling coefficient between the cavity and the bus waveguide.

θ_d= Phase of the coupling coefficient between the cavity and the drop waveguide.

The incoming and outgoing waves can be described as

$$s_{-1} = s_{+2} - e^{-j\theta_{b1}}\sqrt{\frac{\omega_{o1}}{2Q_{b1}}}a \quad (2a)$$

$$s_{-2} = s_{+1} - e^{-j\theta_{b1}}\sqrt{\frac{\omega_{o1}}{2Q_{b1}}}a \quad (2b)$$

$$s_{-3} = -s_{+3} + e^{-j\theta_d}\sqrt{\frac{\omega_{o1}}{Q_d}}a \quad (2c)$$

Let port 1 is the input port and set $s_{+2} = s_{+3} = 0$. Assume that s_{+1} has a $(e^{j\omega t})$ time dependence. Due to the linearity of the system under observation, each wave can be expressed as $x(t) = Xe^{j\omega t}$, where X is the complex amplitude.

Using $a = Ae^{j\omega t}$ and $s_{+1} = S_{+1}e^{j\omega t}$ in Eqn. (1), with $s_{+2} = s_{+3} = 0$, yields

$$A = \frac{e^{j\theta_{b1}}\sqrt{\frac{\omega_{o1}}{2Q_{b1}}}}{j\omega_{o1}(\frac{\omega}{\omega_{o1}}-1)-\frac{\omega_{o1}}{Q_{o1}}-\frac{\omega_{o1}}{2Q_e}}S_{+1} \quad (3a)$$

with

$$Q_e{}^{-1} = Q_{b1}{}^{-1} + Q_d{}^{-1} \quad (3b)$$

Using Eqn. (3a) into Eqns. (2a-c), with $s_{+2} = s_{+2} = 0$, yields the following expressions describing the reflection r_b at the input port, the transmission t_b through the bus, and the transmission t_d through the drop port

$$\mathrm{r}_b \equiv \frac{S_{-1}}{S_{+1}} = -\frac{\frac{1}{2Q_{b1}}}{j(\frac{\omega}{\omega_{o1}}-1)+\frac{1}{Q_{o1}}+\frac{1}{2Q_{b1}}+\frac{1}{2Q_d}} \quad (4a)$$

$$t_b \equiv \frac{S_{-2}}{S_{+1}} = 1 - \frac{\frac{1}{2Q_{b1}}}{j(\frac{\omega}{\omega_{o1}}-1)+\frac{1}{Q_{o1}}+\frac{1}{2Q_{b1}}+\frac{1}{2Q_d}} \quad (4b)$$

$$t_d \equiv \frac{S_{-3}}{S_{+1}} = \frac{e^{j(\theta_{b1}-\theta_d)}\frac{1}{\sqrt{2Q_{b1}Q_d}}}{j(\frac{\omega}{\omega_{o1}}-1)+\frac{1}{Q_{o1}}+\frac{1}{2Q_{b1}}+\frac{1}{2Q_d}} \quad (4c)$$

2.2. Analysis of Wavelength-Selective Reflection Cavity

Figure 4 shows the basic structure of a feedback cavity side coupled to a bus waveguide. It is assumed that both the

cavity and bus waveguide support single mode in the frequency range of interest with negligible nonlinear optics effect. The cavity possesses mirror reflection symmetry with respect to the reference plane. The amplitudes of the incoming waves are denoted by s_{+1} and s_{+2}. The amplitudes of outgoing waves are denoted by s_{-1} and s_{-2}.

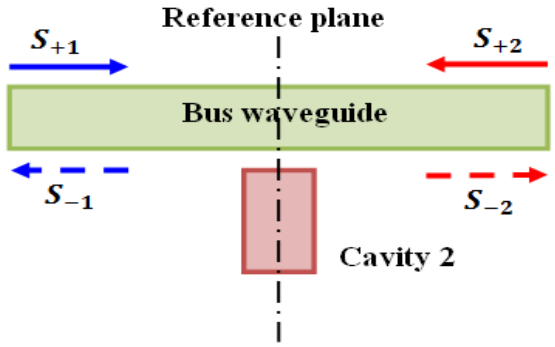

Figure 4. Basic structure of a waveguide side-coupled to cavity 2 which is used to realize the wavelength-selective reflection function

The equation of the resonant mode in the cavity in time is given by [15, 19, 20]

$$\frac{db}{dt} = (j\omega_{o2} - \frac{\omega_{o2}}{Q_{o2}} - \frac{\omega_{o2}}{2Q_{b2}})b + e^{j\theta_{b2}}\sqrt{\frac{\omega_{o2}}{2Q_{b2}}}S_{+1} + e^{j\theta_{b2}}\sqrt{\frac{\omega_{o2}}{2Q_{b2}}}S_{+2} \quad (5)$$

where

b = Cavity field amplitude.

ω_{o2}= Resonance frequency of the cavity.

Q_{o2}= Quality factor due to intrinsic loss.

Q_{b2}= Quality factor due to the rate of decay into the bus waveguide.

θ_{b2}= Phase of the coupling coefficient between the cavity and the bus waveguide.

The outgoing waves are given by

$$s_{-1} = s_{+2} - e^{-j\theta_{b2}}\sqrt{\frac{\omega_{o2}}{2Q_{b2}}}b \quad (6a)$$

$$s_{-2} = s_{+1} - e^{-j\theta_{b2}}\sqrt{\frac{\omega_{o2}}{2Q_{b2}}}b \quad (6b)$$

Let the input signal has ($e^{j\omega t}$) time dependence. Using $s_{+1} = S_{+1}e^{j\omega t}$, $b = Be^{j\omega t}$ and assuming the input signal is applied at port 1 (i.e., $s_{+2} = 0$) then Eqn. (5) gives

$$B = \frac{e^{j\theta_{b2}}\sqrt{\frac{\omega_{o2}}{2Q_{b2}}}}{j(\omega-\omega_{o2})-\frac{\omega_{o2}}{Q_{o2}}-\frac{\omega_{o2}}{2Q_{b2}}}S_{+1} \quad (7)$$

Substituting Eqn. (7) into Eqns. (6a) and (6b) yields the reflection and transmission coefficients, respectively

$$\mathrm{r}_b \equiv \frac{S_{-1}}{S_{+1}} = -\frac{\frac{1}{2Q_{b2}}}{j\left(\frac{\omega}{\omega_{o2}}-1\right)+\frac{1}{Q_{o2}}+\frac{1}{2Q_{b2}}} \quad (8a)$$

$$t_b \equiv \frac{S_{-2}}{S_{+1}} = \frac{j\left(\frac{\omega}{\omega_{o2}}-1\right)+\frac{1}{Q_{o2}}}{j\left(\frac{\omega}{\omega_{o2}}-1\right)+\frac{1}{Q_{o2}}+\frac{1}{2Q_{b2}}} \quad (8b)$$

When the excitation frequency equals the cavity resonance frequency (i.e., $\omega = \omega_{o2}$), then Eqns. (8a) and (8b) reduce to Eqns. (9a) and (9b), respectively

$$\mathrm{r}_o = -\frac{1}{1+2(\frac{Q_{b2}}{Q_{o2}})} \quad (9a)$$

$$t_o = \frac{2(\frac{Q_{b2}}{Q_{o2}})}{1+2(\frac{Q_{b2}}{Q_{o2}})} \quad (9b)$$

When $Q_{o2} \gg Q_{b2}$, then r_o and t_o tend to 1 and 0, respectively.

The full-width at half-maximum (FWHM) of the reflection spectrum can be obtained after finding the half power cut-off frequencies

$$|\mathrm{r}(\omega)|^2 = \frac{1}{2}|\mathrm{r}_o|^2 \quad (10)$$

Using Eqns. (8a) and (9a) yields

$$\left(\frac{\omega}{\omega_{o2}}-1\right)^2 = \left[\frac{1}{Q_{b2}}-\frac{1}{2Q_{o2}}\right]^2$$

$$\frac{\omega}{\omega_{o2}}-1 = \pm\left(\frac{1}{Q_{b2}}-\frac{1}{2Q_{o2}}\right) \quad (11)$$

The plus (minus) sign in Eqn. (11) is associated with the upper (lower) cut-off frequency

$$\omega_h = \omega_{o2} + [\frac{1}{Q_{b2}}-\frac{1}{2Q_{o2}}]\omega_{o2} \quad (12a)$$

$$\omega_l = \omega_{o2} - [\frac{1}{Q_{b2}}-\frac{1}{2Q_{o2}}]\omega_{o2} \quad (12b)$$

The FWHM is given by $\sigma = \omega_h - \omega_l$

$$\sigma = 2\omega_{o2}\left[\frac{1}{Q_{b2}}-\frac{1}{2Q_{o2}}\right] \quad (13a)$$

$$\sigma \cong \frac{\omega_{o2}}{Q_{b2}} \quad \text{when} \quad Q_{o2} \gg Q_{b2} \quad (13b)$$

3. Analysis of Single-Channel Demultiplexer

The single-channel demultiplexer can be represented as two cavities coupled to a waveguide with one drop port. As seen in Figure 5. The cavities 1 and 2 are used to realize resonant tunnelling-based channel drop filterer and wavelength-selective reflection feedback, respectively. The structure can be considered as a three-port network where ports 1, 2, and 3 represent, respectively, the input port, the output port, and the drop port.

The coupled-mode theory can be used to describe the time evaluation of the resonant modes as follows [13-16, 19]

$$\frac{da}{dt} = (j\omega_{o1} - \frac{\omega_{o1}}{Q_{o1}} - \frac{\omega_{o1}}{2Q_{b1}} - \frac{\omega_{o1}}{2Q_d})a + e^{j\theta_{b1}}\sqrt{\frac{\omega_{o1}}{2Q_{b1}}}s_{+1} + e^{j\theta_{b1}}\sqrt{\frac{\omega_{o1}}{2Q_{b1}}}s`_{+1} + e^{j\theta_d}\sqrt{\frac{\omega_{o1}}{Q_d}}s_{+3} \quad (14a)$$

$$\frac{db}{dt} = (j\omega_{o2} - \frac{\omega_{o2}}{Q_{o2}} - \frac{\omega_{o2}}{2Q_{b2}})b + e^{j\theta_{b2}}\sqrt{\frac{\omega_{o2}}{2Q_{b2}}}s_{+2} + e^{j\theta_2}\sqrt{\frac{\omega_{o2}}{2Q_{b2}}}s`_{+2} \quad (14b)$$

where a and b are the resonant mode in cavities 1 and 2, respectively. Further

ω_{o1}= Resonance frequency of cavity 1.

ω_{o2}= Resonance frequency of cavity 2.

Q_{o1}= Quality factor due to intrinsic loss of cavity 1.

Q_{o2}= Quality factor due to intrinsic loss of cavity 2.

Q_{b1}= Quality factor of cavity 1 that is connected with rate of decay into the bus waveguide.

Q_{b2}= Quality factor of cavity 2 that is connected with rate of decay into the bus waveguide.

Q_d= Quality factor of cavity 1 that is related to the rate of decay into the drop waveguide.

θ_{b1}= Phase of the coupling coefficient between cavity 1 and the bus waveguide.

θ_{b2}= Phase of the coupling coefficient between cavity 2 and the bus waveguide.

θ_d= Phase of the coupling coefficient between the cavity 1 and the drop waveguide.

The incoming and outgoing waves can be described as

$$s_{-1} = s`_{+1} - e^{-j\theta_{b1}}\sqrt{\frac{\omega_{o1}}{2Q_{b1}}}a \quad (15a)$$

$$s`_{-1} = s_{+1} - e^{-j\theta_{b1}}\sqrt{\frac{\omega_{o1}}{2Q_{b1}}}a \quad (15b)$$

$$s`_{+1} = s`_{-2}e^{-j\beta D} \quad (15c)$$

$$s_{-2} = s`_{+2} - e^{-j\theta_{b2}}\sqrt{\frac{\omega_{o2}}{2Q_{b2}}}b \quad (15d)$$

$$s`_{-2} = s_{+2} - e^{-j\theta_{b2}}\sqrt{\frac{\omega_{o2}}{2Q_{b2}}}b \quad (15e)$$

$$s`_{+2} = s`_{-1}e^{-j\beta D} \quad (15f)$$

$$s_{-3} = -s_{+3} + e^{-j\theta_d}\sqrt{\frac{\omega_{o1}}{Q_d}}a \quad (15g)$$

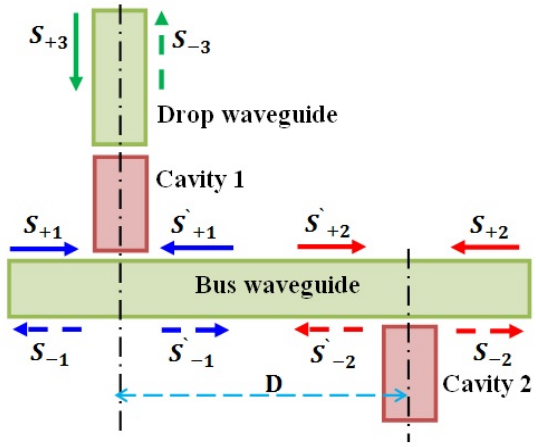

Figure 5. Schematic diagram of demultiplexer filter based on the resonant tunneling effect of the cavity (i.e., Cavity 1) near a bus waveguide with a side-coupled reflection cavity (i.e., Cavity 2)

If the optical signal is applied at port 1 only (i.e., is $s_{+2} = s_{+3} = 0$), then the optical scattering coefficient can be expressed as (see Appendix for details)

$$T_r \equiv \left|\frac{S_{-1}}{S_{+1}}\right|^2 =$$

$$\left|-V(\cos\emptyset - j\sin\emptyset) - 12Qb1[1-V\cos\emptyset - j\sin\emptyset]2j\omega\omega o1 - 1 + V2Qb1\sin\emptyset + 1Qo1 + 12Qd + 12Qb1(1-V\cos\emptyset))2\right| \quad (16a)$$

$$T_b \equiv \left|\frac{S_{-2}}{S_{+1}}\right|^2 =$$

$$\left|(1-V)\left(1 - \frac{\frac{1}{2Q_{b1}}\left[1 - V\left(\cos\cos\varnothing - j\sin\sin\varnothing\right)\right]}{j\left(\frac{\omega}{\omega_{o1}} - 1 + \frac{V}{2Q_{b1}}\sin\sin\varnothing\right) + \frac{1}{Q_{o1}} + \frac{1}{2Q_d} + \frac{1}{2Q_{b1}}\left(1 - V\cos\cos\varnothing\right)}\right)e^{-j\varnothing/2}\right|^2 \quad (16b)$$

$$T_d \equiv \left|\frac{S_{-3}}{S_{+1}}\right|^2 = \left|\frac{e^{j(\theta_{b1}-\theta_d)}\frac{1}{\sqrt{2Q_{b1}Q_d}}[1-V(\cos\emptyset - j\sin\emptyset)]}{j\left(\frac{\omega}{\omega_{o1}} - 1 + \frac{V}{2Q_{b1}}\sin\emptyset\right) + \frac{1}{Q_{o1}} + \frac{1}{2Q_d} + \frac{1}{2Q_{b1}}(1 - V\cos\emptyset)}\right|^2 \quad (16c)$$

where

$$V = \frac{\frac{1}{2Q_{b2}}}{j\left(\frac{\omega}{\omega_{o2}} - 1\right) + \frac{1}{Q_{o2}} + \frac{1}{2Q_{b2}}} \quad (17a)$$

and

$$\emptyset = 2\beta D \quad (17b)$$

Further,

$\emptyset$= Phase between the two reference planes.

β= Propagation constant of the bus waveguide.

D= Distance between the two reference planes.

It is worthing to introduce the amplitude and power scattering parameters from port j to port i

$$t_{ij} \equiv \frac{S_{-i}}{S_{+j}} \quad (18a)$$

The corresponding power scattering parameters is

$$T_{ij} \equiv |t_{ij}|^2 = |\frac{S_{-i}}{S_{+j}}|^2 \quad (18b)$$

According to this notation system, $T_r = |t_{11}|^2$, $T_b = |t_{21}|^2$, and $T_d = |t_{31}|^2$.

The analysis is carried further to investigate the demultiplexer characteristics when the incoming optical signal is applied at port 2. This is useful to characterise the behaviour of a multi-channel demultiplexer implemented by cascading multi single-channel units. Inserting $S_{+1} = S_{+3} = 0$ in Eqns. (14) and (15) yields (see Appendix for more details)

$$T_{22} \equiv \left|\frac{S_{-2}}{S_{+2}}\right|^2 =$$

$$\left|-V - \frac{\frac{1}{2Q_{b1}}(1-V)^2(\cos\emptyset - j\sin\emptyset)}{j\left(\frac{\omega}{\omega_{o1}} - 1 + \frac{V}{2Q_{b1}}\sin\emptyset\right) + \frac{1}{Q_{o1}} + \frac{1}{2Q_d} + \frac{1}{2Q_{b1}}(1 - V\cos\emptyset)}\right|^2 \quad (19a)$$

$$T_{12} \equiv \left|\frac{S_{-1}}{S_{+2}}\right|^2 =$$

$$\left|(1-V)\left(1-\frac{\frac{1}{2Q_{b1}}\left[1-V\left(\cos\cos\varnothing - j\sin\sin\varnothing\right)\right]}{j\left(\frac{\omega}{\omega_{o1}}-1+\frac{V}{2Q_{b1}}\sin\sin\varnothing\right)+\frac{1}{Q_{o1}}+\frac{1}{2Q_d}+\frac{1}{2Q_{b1}}\left(1-V\cos\cos\varnothing\right)}\right)e^{-j\varnothing/2}\right|^2 \quad (19b)$$

$$T_{32} \equiv \left|\frac{S_{-3}}{S_{+2}}\right|^2 =$$

$$\left|-\frac{e^{j(\theta_{b1}-\theta_d)}\frac{1}{\sqrt{2Q_{b1}Q_d}}[1-V(\cos\varnothing/2-j\sin\varnothing/2)]}{j\left(\frac{\omega}{\omega_{o1}}-1+\frac{V}{2Q_{b1}}\sin\varnothing\right)+\frac{1}{Q_{o1}}+\frac{1}{2Q_d}+\frac{1}{2Q_{b1}}(1-V\cos\varnothing)}\right|^2 \quad (19c)$$

4. Analysis of Multi-Channel Demultiplexer

The aim of this section is to compute the scattering parameters of a multi-channel demultiplexer constructed by cascading single-channel demultiplexers (see Fig. 6(a)). In this figure, the forward and backward fields are presented by A_i (solid lines) and B_i (dashed lines), respectively. The ith stage of this configuration corresponds to the ith channel demultiplexer DeMux_i.

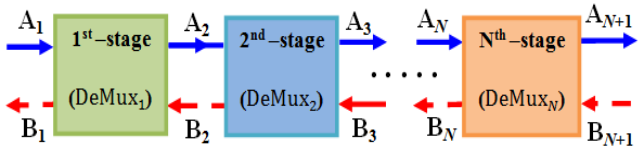

(a)

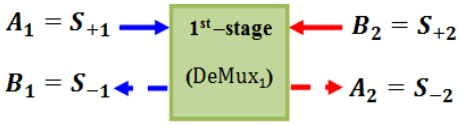

(b)

Figure 6. (a) Block diagram of an N-channel cascade demultiplexer showing the forward fields (A) and backward fields (B). The drop ports are not shown for purpose of clarity. (b) The first channel demultiplexer

Figure 6(b) illustrates the relation between the notations of fields adopted here (A and B) and the scattering field notations for DeMux_1. Here $A_1 = S_{+1}$, $A_2 = S_{-2}$, $B_1 = S_{-1}$, and $B_2 = S_{+2}$. This stage can be described using the concept of scattering matrix

$$\boldsymbol{T_1} = \begin{bmatrix} t_{11} & t_{12} \\ t_{21} & t_{22} \end{bmatrix} \quad (20a)$$

$$S_{-1} = t_{11}S_{+1} + t_{12}S_{+2} \quad (20b)$$

$$S_{-2} = t_{21}S_{+1} + t_{22}S_{+2} \quad (20c)$$

Setting $S_{+2} = 0$ yields

$$t_{11} \equiv \frac{S_{-1}}{S_{+1}} = -V(\cos\varnothing - j\sin\varnothing) - \frac{\frac{1}{2Q_{b1}}[1-V(\cos\varnothing - j\sin\varnothing)]^2}{j\left(\frac{\omega}{\omega_{o1}}-1+\frac{V}{2Q_{b1}}\sin\varnothing\right)+\frac{1}{Q_{o1}}+\frac{1}{2Q_d}+\frac{1}{2Q_{b1}}(1-V\cos\varnothing)} \quad (21a)$$

$$t_{21} \equiv \frac{S_{-2}}{S_{+1}} = (1-V)(1 - \frac{\frac{1}{2Q_{b1}}[1-V(\cos\varnothing - j\sin\varnothing)]}{j\left(\frac{\omega}{\omega_{o1}}-1+\frac{V}{2Q_{b1}}\sin\varnothing\right)+\frac{1}{Q_{o1}}+\frac{1}{2Q_d}+\frac{1}{2Q_{b1}}(1-V\cos\varnothing)})e^{-j\varnothing/2} \quad (21b)$$

when S_{+1} is set to zero

$$t_{12} = \frac{S_{-1}}{S_{+2}} = (1-V)(1 - \frac{\frac{1}{2Q_{b1}}[1-V(\cos\varnothing - j\sin\varnothing)]}{j\left(\frac{\omega}{\omega_{o1}}-1+\frac{V}{2Q_{b1}}\sin\varnothing\right)+\frac{1}{Q_{o1}}+\frac{1}{2Q_d}+\frac{1}{2Q_{b1}}(1-V\cos\varnothing)})e^{-j\varnothing/2} \quad (21c)$$

$$t_{22} = \frac{S_{-2}}{S_{+2}} = -V - \frac{\frac{1}{2Q_{b1}}(1-V)^2(\cos\varnothing - j\sin\varnothing)}{j\left(\frac{\omega}{\omega_{o1}}-1+\frac{V}{2Q_{b1}}\sin\varnothing\right)+\frac{1}{Q_{o1}}+\frac{1}{2Q_d}+\frac{1}{2Q_{b1}}(1-V\cos\varnothing)} \quad (21d)$$

From Eqn. (20b)

$$S_{+2} = \frac{-t_{11}}{t_{12}}S_{+1} + \frac{1}{t_{12}}S_{-1} \quad (22a)$$

Substituting Eqn. (22a) into Eqn. (20b) yields

$$S_{-2} = \left(t_{21} - \frac{t_{11}}{t_{12}}\right)S_{+1} + \frac{t_{22}}{t_{12}}S_{-1} \quad (22b)$$

Equations (22a) and (22b) describe the relation between the fields at port 1 with those at port 2. These two equations can be combined in a matrix representation

$$\begin{bmatrix} A_2 \\ B_2 \end{bmatrix} = \boldsymbol{Q_1}\begin{bmatrix} A_1 \\ B_1 \end{bmatrix} \quad (23a)$$

where

$$\boldsymbol{Q_1} = \begin{bmatrix} q_{11} & q_{12} \\ q_{21} & q_{22} \end{bmatrix} \quad (23b)$$

Note that the matrix $\boldsymbol{Q_1}$ relates the fields at port 2 to those at port 1. The elements of the matrix $\boldsymbol{Q_1}$ are

$$q_{11} = t_{21} - \frac{t_{22}t_{11}}{t_{12}} \quad (24a)$$

$$q_{12} = \frac{t_{22}}{t_{12}} \quad (24b)$$

$$q_{21} = -\frac{t_{11}}{t_{12}} \quad (24c)$$

$$q_{22} = \frac{1}{t_{12}} \quad (24d)$$

Similarly, for the ith demultiplexer

$$\begin{bmatrix} A_{i+1} \\ B_{i+1} \end{bmatrix} = \boldsymbol{Q_i}\begin{bmatrix} A_i \\ B_i \end{bmatrix} \quad (25)$$

For N-channel demultiplexer, the field at the $(N+1)$th port is related to the fields at port 1 by

$$\begin{bmatrix} A_{N+1} \\ B_{N+1} \end{bmatrix} = \boldsymbol{Q_T}\begin{bmatrix} A_1 \\ B_1 \end{bmatrix} \quad (26a)$$

where

$$\boldsymbol{Q_T} = \begin{bmatrix} Q_{11} & Q_{12} \\ Q_{21} & Q_{22} \end{bmatrix} = \prod_{i=1}^{N} \boldsymbol{Q_i} \tag{26b}$$

When the optical signal is applied at port 1 (i.e., $B_{N+1} = 0$), then the reflection and transmission coefficients can be expressed as

$$t_r \equiv \frac{B_1}{A_1} = -\frac{Q_{21}}{Q_{22}} \tag{27a}$$

$$t_b \equiv \frac{A_{N+1}}{A_1} = Q_{11} - \frac{Q_{12}Q_{21}}{Q_{22}} \tag{27b}$$

It is clear from the above analysis that when the optical signal is applied at port 1 of the N-channel demultiplexer, then the fields at the output port ((N+1)th port) will be known (A_{N+1} from Eqn. (27b) and $B_{N+1} = 0$). Then one can go in opposite direction from port (N+1) to port 1 to determine the field components A_i and B_i for each demultiplexer unit. For example, for the Nth channel demultiplexer

$$\begin{bmatrix} A_N \\ B_N \end{bmatrix} = \boldsymbol{Q_N}^{-1} \begin{bmatrix} A_{N+1} \\ B_{N+1} \end{bmatrix} \tag{28a}$$

For the ith channel demultiplexer

$$\begin{bmatrix} A_i \\ B_i \end{bmatrix} = \left[\prod_{j=N}^{i} \boldsymbol{Q_j}^{-1}\right] \begin{bmatrix} A_{N+1} \\ B_{N+1} \end{bmatrix} \tag{28b}$$

Note that $B_{N+1} = 0$ for the case under observation.

The above analysis can be extended further to calculate the signal waves at the drop ports. Let the drop port of the ith demultiplexer is denoted by d_i (see Fig. 7). Note that $S_{+1} = A_i$, $S_{-1} = B_i$, $S_{+(i+1)} = B_{i+1}$, and $S_{-(i+1)} = A_{i+1}$.

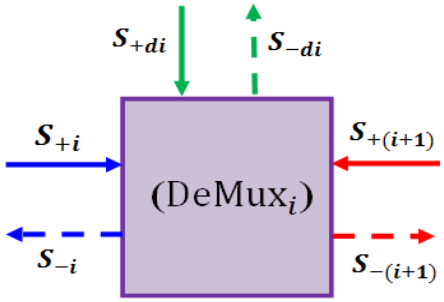

Figure 7. Basic description of the single-channel demultiplexer including the drop port

Under the assumption that no signal is coming to port d_i (i.e., $S_{+d_i} = 0$), then

$$S_{-d_i} = d_{1i}S_{+i} + d_{2i}S_{+(i+1)} \tag{29a}$$

or

$$S_{-d_i} = d_{1i}A_i + d_{2i}B_{(i+1)} \tag{29b}$$

Then

$$d_{1i} \equiv \frac{S_{-d_i}}{S_{+i}}\Big|_{S_{+(i+1)=0}} = \frac{e^{j(\theta_{b1}-\theta_d)}\frac{1}{\sqrt{2Q_{b1}Q_d}}[1-V(\cos\emptyset - j\sin\emptyset)]}{j\left(\frac{\omega}{\omega_{o1}}-1+\frac{V}{2Q_{b1}}\sin\emptyset\right)+\frac{1}{Q_{o1}}+\frac{1}{2Q_d}+\frac{1}{2Q_{d1}}(1-V\cos\emptyset)} \tag{29c}$$

$$d_{2i} \equiv \frac{S_{-d_i}}{S_{+(i+1)}}\Big|_{S_{+i=0}} = \frac{e^{j(\theta_{b1}-\theta_d)}\frac{1}{\sqrt{2Q_{b1}Q_d}}[1-V(\cos\emptyset/2 - j\sin\emptyset/2)]}{j\left(\frac{\omega}{\omega_{o1}}-1+\frac{V}{2Q_{b1}}\sin\emptyset\right)+\frac{1}{Q_{o1}}+\frac{1}{2Q_d}+\frac{1}{2Q_{b1}}(1-V\cos\emptyset)} \tag{29d}$$

5. Simulation Results

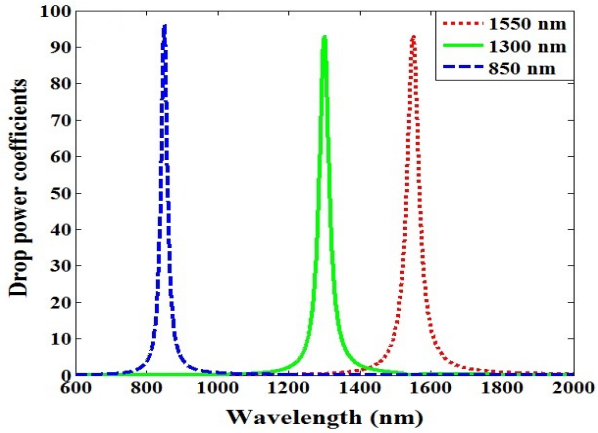

(a)

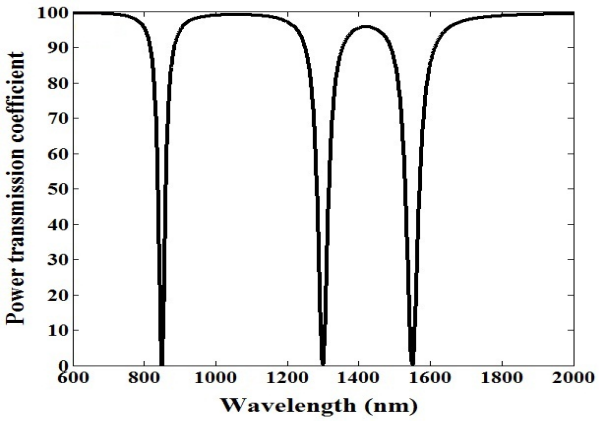

(b)

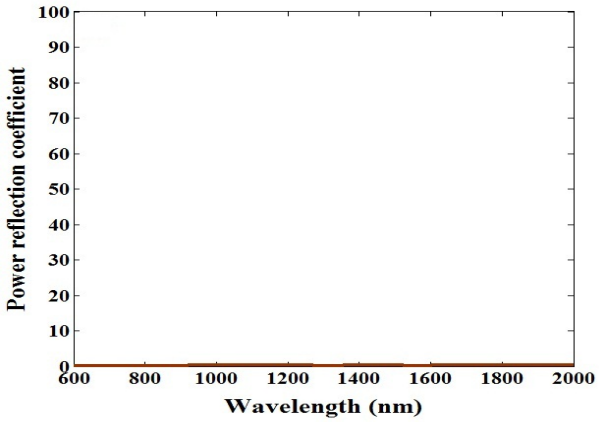

(c)

Figure 8. Power spectra associated with the (1550, 1300, 850 nm) demultiplexer. (a) Drop efficiency at each of the three ports. (b) Power transmission coefficient at the output port. (c) Power reflection coefficient at the input port

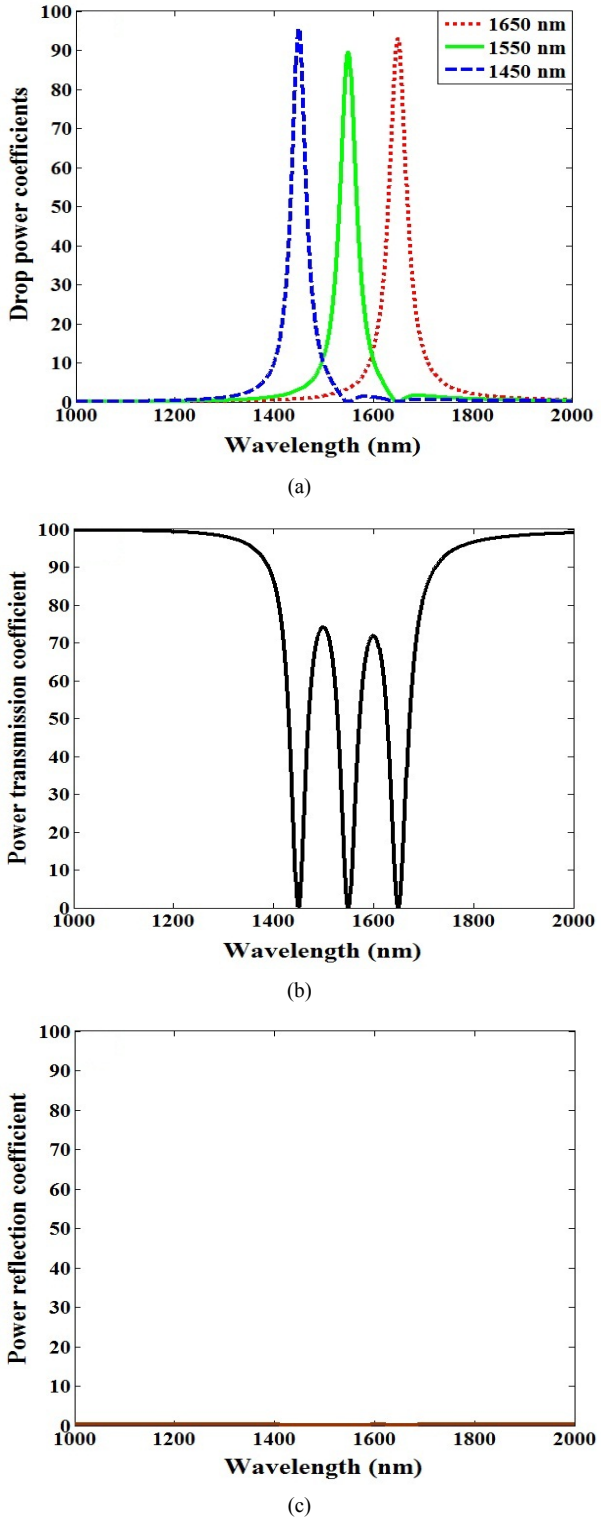

Figure 9. Power spectra associated with the (1650, 1550, 1450 nm) demultiplexer. (a) Drop efficiency at each of the three ports. (b) Power transmission coefficient at the output port. (c) Power reflection coefficient at the input port

Simulation results are presented for two three-channel demultiplexers, (1550, 1300, 850 nm) and (1650, 1550, 1450 nm). The parameters values used in the simulation are Q_{o1} =2200, Q_{o2} =2200, Q_{b1} =80, Q_{b2} =80, and Q_d =40. Further, $\beta D = n\pi$.

The spectral characteristics of the two demultiplexers are displayed in Figs. 8 and 9, respectively. Each figure contains three parts with part "a" displays the drop efficiency at each of the three ports. Parts "b" and "c" show, respectively, the power transmission coefficient at the demultiplexer output port and the power reflection coefficient at the demultiplexer input port. Comparing the result in Fig. 8(a) and Fig. 9(a) reveals the effect of the channel spacing on the drop efficiency.

6. Conclusions

This paper has presented a methodology for the analysis of a multi-channel WDM demultiplexer incorporating cascaded stages. The scattering parameters of each stage have been derived using CMT and the results have been used to characterise the performance of the multi-channel demultiplexer using signal flow transformation. The analysis can be used as a guideline to address the effect of interference between adjacent channels in WDM demultiplexers.

Appendix

Derivation of Transmission Coefficients of the Single-Cannel Demultiplexer

The single-channel demultiplexer under investigation consists of two cavities laterally coupled to a bus waveguide. The demultiplexer is treated as a three-port network as illustrated in section 3 and its characteristics is governed by Eqns. (14) and (15). The aim of this appendix is to derive the transmission coefficient of the demultiplexer when the signal is incident only at port 1 (forward-incident signal) or port 2 (backward-incident signal).

a. Forward-Incident Signal

Set $s_{+2} = s_{+3} = 0$, and let s_{+1}, a, and b have a $(e^{j\omega t})$ time dependence. then from Eqns. (14a) and (14b) one gets

$$j\omega A = \left(j\omega_{o1} - \frac{\omega_{o1}}{Q_{o1}} - \frac{\omega_{o1}}{2Q_{b1}} - \frac{\omega_{o1}}{2Q_d}\right)A + e^{j\theta_{b1}}\sqrt{\frac{\omega_{o1}}{2Q_{b1}}}S_{+1} + e^{j\theta_{b1}}\sqrt{\frac{\omega_{o1}}{2Q_{b1}}}S`_{+1} \quad \text{(A1)}$$

$$j\omega B = \left(j\omega_{o2} - \frac{\omega_{o2}}{Q_{o2}} - \frac{\omega_{o2}}{2Q_{b2}}\right)B + e^{j\theta_{b2}}\sqrt{\frac{\omega_{o2}}{2Q_{b2}}}S`_{+2} \quad \text{(A2)}$$

Simplifying Eqn. (A2), one gets

$$B = \frac{e^{j\theta_{b2}}\sqrt{\frac{\omega_{o2}}{2Q_{b2}}}}{j(\omega-\omega_{o2})+\frac{\omega_{o2}}{Q_{o2}}+\frac{\omega_{o2}}{2Q_{b2}}}S`_{+2} \quad \text{(A3)}$$

Substituting Eqn. (15e) into Eqn. (15c) yields

$$S`_{+1} = (S_{+2} - e^{-j\theta_{b2}}\sqrt{\frac{\omega_{o2}}{2Q_{b2}}}B)e^{-j\beta D} \quad \text{(A4)}$$

Substituting Eqn. (A3) into Eqn. (A4) yields

$$S`_{+1} = -Ve^{-j\beta D}S`_{+2} \quad \text{(A5)}$$

where

$$V = \frac{\frac{1}{2Q_{b2}}}{j(\frac{\omega}{\omega_{o2}}-1)+\frac{1}{Q_{o2}}+\frac{1}{2Q_{b2}}} \quad (16a)$$

Substituting Eqn. (15b) into Eqn. (15f) yields

$$S`_{+2} = (S_{+1} - e^{-j\theta_{b1}}\sqrt{\frac{\omega_{o1}}{2Q_{b1}}}A)e^{-j\beta D} \quad (A6)$$

Substituting Eqn. (A6) into Eqn. (A5) yields

$$S`_{+1} = -V(S_{+1} - e^{-j\theta_{b1}}\sqrt{\frac{\omega_{o1}}{2Q_{b1}}}A)e^{-j\emptyset} \quad (A7)$$

Substituting Eqn. (A7) into Eqn. (A1) and using $e^{-j\emptyset} = \cos\emptyset - j\sin\emptyset$, one gets

$$A = \frac{e^{-j\theta_{b1}}\sqrt{\frac{\omega_{o1}}{2Q_{b1}}}(1-V(\cos\emptyset - j\sin\emptyset))}{j\,\omega_{o1}\left(\frac{\omega}{\omega_{o1}}-1+\frac{V}{2Q_{b1}}\sin\emptyset\right)+\frac{\omega_{o1}}{Q_{o1}}+\frac{\omega_{o1}}{2Q_d}+\frac{\omega_{o1}}{2Q_{b1}}(1-V\cos\emptyset)}S_{+1} \quad (A8)$$

Substituting Eqns. (A7) and (A8) into Eqn. (15a) yields

$$\frac{S_{-1}}{S_{+1}} = -V(\cos\emptyset - \mathrm{j}\sin\emptyset) - \frac{\frac{1}{2Q_{b1}}(1-V(\cos\emptyset - j\sin\emptyset))^2}{j\left(\frac{\omega}{\omega_{o1}}-1+\frac{V}{2Q_{b1}}\sin\emptyset\right)+\frac{1}{Q_{o1}}+\frac{1}{2Q_d}+\frac{1}{2Q_{b1}}(1-V\cos\emptyset)} \quad (A9)$$

Taking absolute and square to Eqn. (A9), one gets Eqn. (16a).

Substituting Eqn. (A3) into Eqn. (15d) yields

$$S_{-2=}(1-V)S`_{+2} \quad (A10)$$

Substituting Eqns. (A6) and (A8) into Eqn. (A10) yields

$$\frac{S_{-2}}{S_{+1}} = (1-V)\left(1 - \frac{\frac{1}{2Q_{b1}}(1-V(\cos\emptyset - j\sin\emptyset))}{j\left(\frac{\omega}{\omega_{o1}}-1+\frac{V}{2Q_{b1}}\sin\emptyset\right)+\frac{1}{Q_{o1}}+\frac{1}{2Q_d}+\frac{1}{2Q_{b1}}(1-V\cos\emptyset)}\right)e^{-j\emptyset/2} \quad (A11)$$

Taking absolute and square to Eqn. (A11), one gets Eqn. (16b).

Substituting Eqn. (A8) into Eqn. (15g) yields

$$\frac{S_{-3}}{S_{+1}} = \frac{e^{j(\theta_{b1}-\theta_d)}\frac{1}{\sqrt{2Q_{b1}Q_d}}(1-V(\cos\emptyset - j\sin\emptyset))}{j\left(\frac{\omega}{\omega_{o1}}-1+\frac{V}{2Q_{b1}}\sin\emptyset\right)+\frac{1}{Q_{o1}}+\frac{1}{2Q_d}+\frac{1}{2Q_{b1}}(1-V\cos\emptyset)} \quad (A12)$$

Taking the square of the absolute value of Eqn. (A12) gives Eqn. (16c).

b. Backward-Incident Signal

Set $s_{+1} = s_{+3} = 0$, and let s_{+2} has a ($e^{j\omega t}$) time dependence, then from Eqns. (14a) and (14b) one gets

$$j\omega A = \left(j\omega_{o1} - \frac{\omega_{o1}}{Q_{o1}} - \frac{\omega_{o1}}{2Q_{b1}} - \frac{\omega_{o1}}{2Q_d}\right)A + e^{j\theta_{b1}}\sqrt{\frac{\omega_{o1}}{2Q_{b1}}}S`_{+1} \quad (A13)$$

$$B = \frac{e^{j\theta_{b2}}\sqrt{\frac{\omega_{o2}}{2Q_{b2}}}}{j(\omega-\omega_{o2})+\frac{\omega_{o2}}{Q_{o2}}+\frac{\omega_{o2}}{2Q_{b2}}}S_{+2} + \frac{e^{j\theta_{b2}}\sqrt{\frac{\omega_{o2}}{2Q_{b2}}}}{j(\omega-\omega_{o2})+\frac{\omega_{o2}}{Q_{o2}}+\frac{\omega_{o2}}{2Q_{b2}}}S`_{+2} \quad (A14)$$

Substituting Eqn. (A14) into Eqn. (A4) yields

$$S`_{+1} = \left((1-V)S_{+2} - VS`_{+2}\right)e^{-j\beta D} \quad (A15)$$

Substituting Eqn. (A6) into Eqn. (A15) yields

$$S`_{+1} = (1-V)e^{-j\beta D}S_{+2} + Ve^{-j\emptyset}e^{-j\theta_{b1}}\sqrt{\frac{\omega_{o1}}{2Q_{b1}}}A \quad (A16)$$

Substituting Eqn. (A16) into Eqn. (A13) and using $e^{-j\emptyset} = \cos\emptyset - j\sin\emptyset$ one gets

$$A = \frac{e^{-j\theta_{b1}}\sqrt{\frac{\omega_{o1}}{2Q_{b1}}}(1-V(\cos(\emptyset/2) - j\sin(\emptyset/2)))}{j\,\omega_{o1}\left(\frac{\omega}{\omega_{o1}}-1+\frac{V}{2Q_{b1}}\sin\emptyset\right)+\frac{\omega_{o1}}{Q_{o1}}+\frac{\omega_{o1}}{2Q_d}+\frac{\omega_{o1}}{2Q_{b1}}(1-V\cos\emptyset)}S_{+2} \quad (A17)$$

Substituting Eqn. (A14) into Eqn. (15d) yields

$$S_{-2} = (1-V)S`_{+2} - VS_{+2} \quad (A18)$$

Substituting Eqns. (A6) and (A17) into Eqn. (A18) yields

$$\frac{S_{-2}}{S_{+2}} = -V - \frac{\frac{1}{2Q_{b1}}(1-V)^2(\cos\emptyset - j\sin\emptyset)}{j\left(\frac{\omega}{\omega_{o1}}-1+\frac{V}{2Q_{b1}}\sin\emptyset\right)+\frac{1}{Q_{o1}}+\frac{1}{2Q_d}+\frac{1}{2Q_{b1}}(1-V\cos\emptyset)} \quad (A19)$$

Taking absolute and square to Eqn. (A19), one gets Eqn. (19a).

Substituting Eqns. (A16) and (A17) into Eqn. (15a) yields

$$\frac{S_{-1}}{S_{+2}} = (1-V)\left(1 - \frac{\frac{1}{2Q_{b1}}(V(\cos\emptyset - j\sin\emptyset)-1}{j\left(\frac{\omega}{\omega_{o1}}-1+\frac{V}{2Q_{b1}}\sin\emptyset\right)+\frac{1}{Q_{o1}}+\frac{1}{2Q_d}+\frac{1}{2Q_{b1}}(1-V\cos\emptyset)}\right)e^{-j\emptyset/2} \quad (A20)$$

Taking absolute and square to Eqn. (A20), one gets Eqn. (19b).

Substituting Eqn. (A17) into Eqn. (15g) yields

$$\frac{S_{-3}}{S_{+2}} = \frac{e^{j(\theta_{b1}-\theta_d)}\frac{1}{\sqrt{2Q_{b1}Q_d}}(1-V(\cos(\emptyset/2) - j\sin(\emptyset/2)))}{j\left(\frac{\omega}{\omega_{o1}}-1+\frac{V}{2Q_{b1}}\sin\emptyset\right)+\frac{1}{Q_{o1}}+\frac{1}{2Q_d}+\frac{1}{2Q_{b1}}(1-V\cos\emptyset)} \quad (A21)$$

Taking the square of the absolute value of Eqn. (A21) gives Eqn. (19c).

REFERENCES

[1] J. D. Reis, A. Shahpari, R. Ferreira, S. Ziaie, D. M. Neves, M. Lima, and A. L. Teixeira, "Terabit+ (192 × 10 Gb/s) nyquist shaped UDWDM coherent PON with upstream and downstream over a 12.8 nm band", Journal of Lightwave Technology, Vol. 32, No. 4, PP. 729-735, February 2014.

[2] N. Minato, S. Kobayashi, K. Sasaki, and M. Kashima, "Design of hybrid WDM/OCDM add/drop filters and its experimental demonstration for passive routing in metropolitan and access integrated network", Journal of Lightwave Technology, Vol. 32, No. 6, PP. 1120-1131, March 2014.

[3] W. Cui, T. Shao, and J. Yao, "Wavelength reuse in a UWB over WDM-PON based on injection locking of a Fabry–P´erot laser diode and polarization multiplexing", Journal of Lightwave Technology, Vol. 32, No. 2, PP. 220-227, January 2014.

[4] F. Lu, Z. Wang, K. Li, and A. Xu, "A plasmonic triple-wavelength demultiplexing structure based on a MIM waveguide with side-coupled nanodisk cavities", IEEE

Transactions on Nanotechnology, Vol. 12, No. 6, PP. 1185-1190, November 2013.

[5] M. Bahadori, A. Eshaghian, H. Hodaei, M. Rezaei, and K. Mehrany, "Analysis and design of optical demultiplexer based on arrayed plasmonic slot cavities: transmission line model", IEEE Photonics Technology Letters, Vol. 25, No. 8, PP. 784-786, April 2013.

[6] A. Khorshidahmad and A. G. Kirk, "Reflective heterostructure photonic crystal superprism demultiplexer", IEEE Photonics Technology Letters, Vol. 24, No. 4, PP. 303-305, February 2012.

[7] D. Yilmaz, I. Halil Giden, M. Turduev, and H. Kurt, "Design of a wavelength selective medium by graded index photonic crystals", IEEE Journal of Quantum Electronics, Vol. 49, No. 5, PP. 477-484, May 2013.

[8] K. Okamoto, "Wavelength-division-multiplexing devices in thin SOI: advances and prospects", IEEE Journal of Selected Topics in Quantum Electronics, Vol. 20, No. 4, Article Number 8200410, July/August 2014.

[9] M. Piels, J. F. Bauters, M. L. Davenport, M. J. R. Heck, and J. E. Bowers," Low-loss silicon nitride AWG demultiplexer heterogeneously integrated with hybrid III–V/silicon photodetectors", Journal of Lightwave Technology, Vol. 32, No. 4, PP. 817-823, February 2014.

[10] J. Chen, Z. Li, J. Li, and Q. Gong, "Compact and high-resolution plasmonic wavelength demultiplexers based on fano interference", Optics Express, Vol. 19, No. 10, PP. 9976-9985, May 2011.

[11] X. G. Huang and J. Tao, "Nano-plasmonic filters based on tooth-shaped waveguide structures", in "Optical devices in communication and computation", P. Xi (Ed.), Chapter 8, PP. 153-174, InTech, 2012.

[12] I. Zand, M. S. Abrishamian, and T. Pakizeh, "Nanoplasmonic loaded slot cavities for wavelength filtering and demultiplexing", IEEE Journal of Selected Topics in Quantum Electronics, Vol. 19, No. 3, Article Number 4600505, May/June 2013.

[13] H. Ren, C. Jiang, W. Hu, M. Gao, J. Wang, "Photonic crystal channel drop filter with a wavelength-selective reflection micro-cavity", Optics Express Vol. 14, No. 6, PP. 2446-2458, March 2006.

[14] H. Lu, X. Liu, Y. Gong, D. Mao, and L. Wang, "Enhancement of transmission efficiency of nanoplasmonic wavelength demultiplexer based on channel drop filters and reflection nanocavities", Optics Express, Vol. 19, No. 14, PP.12885-12890, July 2011.

[15] H. A. Haus, "Waves and fields in optoelectronics", Prentice-Hall, Inc., Englewood Cliffs, New Jersey, 1984.

[16] C. Manolatou, M. J. Khan, S. Fan, P. R. Villeneuve, H. A. Haus, and J. D. Joannopoulos, "Coupling of modes analysis of resonant channel Add–Drop filters", IEEE Journal of Quantum Electronics, Vol. 35, No. 9, PP. 1322-1331, September 1999.

[17] S. Kim, I. Park, and H. Lim, "Highly efficient photonic crystal-based multichannel drop filters of three-port system with reflection feedback", Optics Express, Vol. 12, No. 22, PP. 5518-5525, November 2004.

[18] J. Zhou, D. Mu, J. Yang, W. Han, and X. Di, "Coupled-resonator-induced transparency in photonic crystal waveguide resonator system", Optics Express, Vol. 19, No. 5, PP. 4856-4861, February 2011.

[19] K. Fasihi and S. Mohammadnejad, "Highly efficient channel-drop filter with a coupled cavity-based wavelength-selective reflection feedback" Optics Express, Vol. 17, No. 11, PP. 8983-8997, May 2009.

[20] D. Park, S. Kim, I. Park, and H. Lim, "Higher order optical resonant filters based on coupled defect resonators in photonic crystals", Journal of Lightwave Technology, Vol. 23, No. 5, PP. 1923-1928, May 2005.